Redox Biology 26 (2019) 101297

Contents lists available at ScienceDirect

Redox Biology

journal homepage: www.elsevier.com/locate/redox

Research Paper

Carbonic anhydrase 9 confers resistance to ferroptosis/apoptosis in malignant mesothelioma under hypoxia

Zan Li[a], Li Jiang[a], Shan Hwu Chew[a], Tasuku Hirayama[b], Yoshitaka Sekido[c], Shinya Toyokuni[a,d,*]

[a] Department of Pathology and Biological Responses, Nagoya University Graduate School of Medicine, 65 Tsurumai-cho, Showa-ku, Nagoya, 466-8550, Japan
[b] Laboratory of Pharmaceutical and Medicinal Chemistry, Gifu Pharmaceutical University, 1-25-4 Daigaku-Nishi, Gifu, 501-1113, Japan
[c] Division of Cancer Biology, Aichi Cancer Center Research Institute, Nagoya, 464-8681, Japan
[d] Sydney Medical School, The University of Sydney, NSW, Australia

ARTICLE INFO

Keywords:
Carbonic anhydrase
Malignant mesothelioma
Iron metabolism
Tumor biology
Apoptosis
Ferroptosis
Catalytic Fe(II)

ABSTRACT

Hypoxia and acidity provide microenvironment for selection under evolutionary pressure and proliferation in cancer cells. Carbonic anhydrases (CAs) are a superfamily of metalloenzymes present in all life kingdoms, equilibrating the reactions among CO_2, bicarbonate and H^+. CA9, a membrane-associated α-CA, has been a drug target for various cancers. Whereas iron is essential not only for cancer cells but also for all the lives on earth, little is known on the association among hypoxia, iron metabolism, extracellular acidity and redox regulation. Malignant mesothelioma (MM), an aggressive tumor with poor prognosis, is an intriguing model in that asbestos-associated pathogenesis includes excess iron environment during carcinogenesis. Re-analysis of rat asbestos-induced MM model revealed an inverse association between high *CA9* expression and survival. Here we used human MMs to identify the molecular events surrounding CA9 from the viewpoint of iron metabolism. *CA9* expression was significantly higher in MM cells than in MeT-5A mesothelial cells, which was further amplified under hypoxia (1%O_2) with increased catalytic Fe(II). CA9 suppression by inhibitors (S4 and U104) decreased viability and migration of MM cells, accompanied by overexpression of TFRC, IREB1/2 and FPN1(SLC40A1) and by downregulation of FTH/FTL. This expressional pattern was similar to that of erastin-induced ferroptosis in the same cells. Furthermore, we observed mitochondrial fission and enhanced autophagy with increased catalytic Fe (II) in both mitochondria and lysosomes after CA9 inhibition, accompanied by increased peroxides, mitochondrial O_2^- and lipid peroxidation. The eventual cell death was significantly inhibited by deferoxamine, ferrostatin-1 and Z-VAD-FMK, suggesting a mixed cell death of ferroptosis and apoptosis. Therefore, CA9 plays a role in equilibrating among hypoxia, iron metabolism and redox regulation in MM cells.

1. Introduction

Cancer is a leading cause of human mortality across the globe [1]. Hypoxia and extracellular acidity provide microenvironment for selection under evolutionary pressure and persistent invasive proliferation in cancer cells [2]. Malignant mesothelioma (MM) is a rare but highly aggressive cancer, exhibiting short median survival (~13 months) [3,4]. MM derives from mesothelial cells, wrapping internal organs and lining the somatic cavities to provide a protective surface and to facilitate intracoelomic movement. Recently, pathogenic mechanisms linking asbestos-exposure [5] and catalytic Fe(II)-induced oxidative stress in MM carcinogenesis have been well established [6,7]. Hemoglobin adsorption on asbestos surface is a key phenomenon causing local iron overload [8–10], eventually leading to oxidative DNA damage in mesothelial cells due to the affinity of asbestos to histones [9,11]. Thus, repeated phlebotomy [12] or local iron removal [13,14] is suggested as a preventive measure against MM after exposure to asbestos, when therapeutic regimens for MM are still dismal [15].

Hypoxia is a microenvironmental hallmark in solid tumors, which is regarded as pO_2 < 10 mmHg (equivalent to < 1.3% O_2 *in vitro*) in comparison to pO_2 of 40–50 mmHg in peritoneal cavity [16]. Mass hypoxic regions have been well recognized in human MM [17,18], which may be endowing MM with various aggressive behaviors, including invasion, high proliferation rate [19] and a resistance to apoptosis [20], based on aberrant activation of a heterodimeric transcription factor, hypoxia inducible factor-1 (HIF-1) [21–23]. Of note, numerous iron metabolism-associated genes [24], including iron transport (*Ex. TFRC* [also as *TfR1*] and *SLC11A2,* encoding transferrin

* Corresponding author. Department of Pathology and Biological Responses, Nagoya University Graduate School of Medicine, 65 Tsurumai-cho, Showa-ku, Nagoya, 466-8550, Japan.
E-mail address: toyokuni@med.nagoya-u.ac.jp (S. Toyokuni).

https://doi.org/10.1016/j.redox.2019.101297
Received 24 June 2019; Received in revised form 30 July 2019; Accepted 7 August 2019
Available online 10 August 2019

Abbreviations

CA9	carbonic anhydrase 9
CTRL	control
DFO	deferoxamine mesylate
DMEM	Dulbecco's modified Eagle's medium
DMSO	dimethyl sulfoxide
EM	epithelioid mesothelioma
FACS	fluorescence activated cell sorter
Fer-1	Ferrostatin-1
FITC	fluorescein isothiocyanate
HIF-1	hypoxia-inducible factor-1
IRP2	iron regulatory protein 2
MM	malignant mesothelioma
MTT	*3-[4,5*-Dimethylthiazol-2-yl]-*2,5*-diphenyltetrazolium bromide
PBS	phosphate-buffered saline
PFA	paraformaldehyde
PI	propidium iodide
ROS	reactive oxygen species
RPMI	Roswell Park Memorial Institute medium
RT	room temperature
SM	sarcomatoid mesothelioma
TUNEL	terminal deoxynucleotidyl transferase-mediated dUTP nick end labeling
WST	*2-(4*-Iodophenyl)-*3-(4*-nitrophenyl)-*5-(2,4*-disulfophenyl)-*2H*-tetrazolium, monosodium salt

receptor and divalent metal transporter-1, respectively) [25–27]; iron storage (*FTH,* encoding ferritin heavy chain) [28] are under control by hypoxia-responsive elements in the promoter region. Hypoxia may up-regulate with a posttranslational mechanism the levels of iron regulatory protein 2 (IRP2), which can regulate the stability of each mRNA differentially to increase for *TFRC* and *SLC11A2* and simultaneously to decrease for *FTH* [29]. Furthermore, recent studies suggest that hypoxia promotes cancer cells to acquire aggressive phenotypes through re-programming iron metabolism for more iron acquisition and retention [30,31]. However, it is still unclear why MM cells under hypoxia continue to show iron addiction without toxicity [7].

Carbonic anhydrases (*CAs*; EC 4.2.1.1) are a superfamily (CA1-16) of metalloenzymes present in all life kingdoms, equilibrating the reactions among CO_2, bicarbonate and H^+ [32]. Carbonic anhydrase 9 (CA9), a membrane-associated α-CA present in fish, rodents and primates [33], has been a drug target for various cancers [34]. *CA9* is an inductively expressed gene in response to hypoxia in cancers [35,36]. In addition to intracellular pH regulation, extracellular acidity by CA9 appears to provide multiple merits for cancer cells [2]. For example, acidic pH can facilitate extracellular matrix remodeling through over-expressing and activating reorganizational proteases, such as matrix metalloproteinases [37], and further may aid evasion of apoptosis by adopting the pro-survival Bcl-2 family expression pattern [38]. CA9 indeed contributes to the migration and invasion of tumor cells through enhancing MMP14-mediated collagen degradation in breast cancer cells [39]; *CA9* overexpression can increase metastatic potential through Rho-GTPase-related epithelial-mesenchymal transition in a cervical cancer cell line [40]; *CA9* overexpression is associated with a reduced *Th1* response and worse overall survival in metastatic melanoma and basal-like breast cancer [41]. In the present study, we used human MM cells to identify the molecular events surrounding CA9 from the viewpoint of iron metabolism, considering a recent report that crocidolite or chrysotile exposure upregulates *CA9* expression in an immortalized mesothelial cell line, MeT-5A [42]. An intimate association of iron metabolism with hypoxia and redox regulation via CA9 was for the first time revealed.

2. Materials and methods

2.1. Cell lines and culture conditions

Human mesothelioma cell lines, ACC-Meso-1 [43], NCI–H2373 and NCI–H2052, provided as gifts from Dr. Adi F. Gazdar, were used. Immortalized human mesothelial cell line, MeT-5A, was purchased from ATCC (Manassas, VA). Cells were cultured with RPMI-1640 (189–02025, Wako, Osaka, Japan) containing 10% fetal bovine serum (Biowest; Nuaillé, France) under 5% CO_2 atmosphere. To generate hypoxic condition, cells were cultured in a Tri-Gas incubator (MCO-5M, PHCbi; Tokyo, Japan) achieved by nitrogen balanced atmosphere (94% N_2, 1% O_2, 5% CO_2).

2.2. Chemicals

CA9 inhibitors, S4 (5577) and U104 (4540) were from Tocris Bioscience (Bristol, UK), which were dissolved in dimethyl sulfoxide (DMSO). Erastin (17754) was from Cayman Chemical (Ann Arbor, MI). Ferrostatin-1 (Fer-1; SML0583) was from Sigma-Aldrich (St. Louis, MO). Z-VAD-FMK (Z-VAD; S7023) was from Selleck. Deferoxamine mesylate (DFO; D9533) was from Sigma Aldrich (St. Louis, MO).

2.3. Antibodies

Mouse monoclonal anti-CA9 antibody (NBP1-51691) was from Novus Biologicals (Centennial, CO). Rabbit monoclonal anti–HIF–1α (ab51608), rabbit polyclonal anti-SLC40A1 (ab58695) and rabbit polyclonal anti-ferritin light chain (ab69090) antibodies were from Abcam (Cambridge, UK). Rabbit polyclonal anti-ferritin heavy chain antibody (sc-25617) was from Santa Cruz Biotechnology (Dallas, TX). Mouse monoclonal anti-transferrin receptor-1 antibody (13–6800) was from Thermo Fisher Scientific (Pittsburg, PA). Rabbit monoclonal anti-IRP1/IRP2 (20272S/37135), rabbit monoclonal anti-LAMP1 (9091), rabbit monoclonal anti-LC3B (3868) and rabbit polyclonal anti-cleaved caspase-3 (9661) antibodies were from Cell Signaling (Danvers, MA). Mouse monoclonal anti-β-actin (A1978) was from Sigma Aldrich.

2.4. RNA isolation and quantitative RT-PCR

Total RNA was isolated from cultured cells by using RNeasy Plus Mini Kit (Qiagen; Hilden, Germany) and reversely transcribed into *c*DNA using SuperScript III First-Strand Synthesis kit (Invitrogen; Carlsbad, CA). Gene expression levels were quantified by Platinum SYBR Green qPCR SuperMix-UDG kit (Invitrogen) by using an Applied Biosystems Model 7300 Real-Time PCR System (Applied Biosystems; Waltham, MA). The mRNA levels were normalized by *GAPDH* (as internal reference) and calculated according to the $2^{-\Delta\Delta CT}$ method [44]. Multiple independent samples were used ($N \geq 3$), each of which was analyzed in duplicate. The primer sequences were as follows: human *CA9*, forward, 5′-GGGTGTCATCTGGACTGTGTT-3′; reverse, 5′- CTTCT GTGCTGCCTTCTCATC-3′ (product size, 309 bp); human *DRP1*, forward, 5′-CCAAGGTGCCTGTAGGTGAT-3′; reverse, 5′-CAGCAGTGACA GCGAGGATA-3′ (108 bp); human *GAPDH*, forward, 5′-CTGACTTCAA CAGCGACACC-3′; reverse, 5′- TAGCCAAATTCGTTGTCATACC-3′ (109 bp).

2.5. Protein extraction and Western blot analysis

Protein lysate was prepared from cultured cells by using an ice-cold cell lysis buffer supplemented with a protease inhibitor cocktail (Roche;

Basel, Switzerland). Protein concentration was measured with a protein assay bicinchoninate kit (Nacalai Tesque, Kyoto, Japan). Western blot analysis was performed as previously described [45]. Detection was performed by using Chemi-Lumi One Ultra Reagent (Nacalai Tesque). The dilution of primary antibodies used was as follows: anti-CA9 (1:2000), anti–HIF–1α (1:1000), anti-transferrin receptor-1 (1:2000), anti-IRP1/IRP2 (1:2000), anti-ferritin light/heavy chain (1:1000), anti-SLC40A1 (1:500), anti-LC3B (1:1000), anti-LAMP-1 (1:1000), anti-cleaved caspase-3 (1:500) and anti-β-actin (1:2000).

2.6. Cell viability assay

Cell viability was accessed either with MTT or WST-1 assay. 2.0×10^3 cells were seeded per well in 96-well plates and incubated for 16 h at 37 °C in normoxia (21% O_2). After treatment with CA9 inhibitors under hypoxia for 24, 48 or 72 h, medium was replaced with fresh serum-free RPMI-1640 containing MTT or WST-1 reagent and incubated in normoxia for 2.5 h at 37 °C. Plates were scanned at 560 nm (MTT) or 450 nm (WST-1) with a Multiscan FC plate reader (Thermo Fisher Scientific).

2.7. Wound healing assay

The cells were seeded in 6-well plates and incubated in normoxia. After reaching confluence, wounds were inflicted by scratching with a sterile pipette tip for 200 μl across the monolayer, when the medium was replaced to remove cell debris. The cells were thereafter incubated under hypoxia with CA9 inhibitors for 24 h. The identical area of wound at the central area was measured at 0 and 24 h time points, respectively. The healing rate was determined by measuring wound ratio between the closure and the original areas, using Photoshop CS6 software (Adobe; San Jose, CA).

2.8. Cellular localization of catalytic Fe(II)

Catalytic Fe(II) was detected with a fluorescent turn-on probe, SiRhoNox-1 (FerroFarRed; Goryo Chemical, Sapporo, Japan), as previously described [46]. Cells (5×10^4) were cultured in normoxia on 35-mm glass bottom dish (Matsunami; Kishiwada, Japan) for 16 h at 37 °C. After treatment with CA9 inhibitors under hypoxia for 48 h, cells were co-stained with 5 μM of SiRhoNox-1 and 200 nM of LysoTracker Green (Thermo Fisher Scientific) in FluoroBrite DMEM (A1896702, Gibco, Thermo Fisher Scientific) for 30 min at 37 °C in normoxia, followed by incubation with 75 nM of MitoTracker Red (Thermo Fisher Scientific) for another 30 min. We confirmed that 1-h incubation in FluoroBrite DMEM containing 0.1 mg/L (0.25 μM) $Fe(NO_3)_3$ scarcely affects iron metabolism of the cells within this limited period. Medium was replaced with new FluoroBrite DMEM, followed by observation with a confocal microscope (LSM880, Carl Zeiss; Oberkochen, Germany). The excitation/emission used for SiRhoNox-1, LysoTracker and MitoTracker probes were 633/670, 504/511 and 579/599 nm, respectively. Local signal intensity of the regions overlapped with each organelle-trackers were analyzed with ZEN Imaging Software (Carl Zeiss).

2.9. Immunofluorescence

Cells (5×10^4) were cultured in normoxia on 35-mm glass bottom dish for 16 h at 37 °C. After treatment with CA9 inhibitors under hypoxia for 48 h, cells were stained with MitoTracker Red in FluoroBrite DMEM for 30 min in normoxia. Cells were then washed and fixed with 4% (w/v) paraformaldehyde for 10 min at room temperature RT), followed by incubation with ice-cold acetone for 5 min at RT. Blocking was performed with 10% goat-serum in phosphate-buffered saline (PBS) for 1 h at RT. The cells were then incubated with the primary antibody against LC3B (1:1000) in 3% bovine serum albumin at RT, washed 3 times with PBS and then incubated with the secondary antibody, goat anti-rabbit IgG (1:500) conjugated with Alexa Fluor 647 (Invitrogen) for 1 h at RT. LSM880 (Carl Zeiss) was used to analyze intensity and co-localization.

2.10. Terminal deoxynucleotidyl transferase-mediated dUTP nick end labeling (TUNEL) assay

After treatment with CA9 inhibitors under hypoxia for 48 h, cells were fixed with 4% paraformaldehyde for 10 min at RT and washed 3 times by PBS. TUNEL assay was performed, using apoptosis *in situ* detection kit (Wako) according to the manufacturer's protocol, followed by detection with a light microscope.

2.11. Detection of ROS

After inhibition of CA9 in MM cells under hypoxia or 48 h, cellular ROS levels were evaluated by staining with 5 μM of CM-H2DCFDA (Thermo Fisher Scientific, C6827) and with 5 μM of MitoSOX (Thermo Fisher Scientific, M36008); lipid peroxidation was quantified by incubating with BODIPY C11 (Thermo Fisher Scientific, D3861) in FluoroBrite DMEM for 30 min in normoxia at 37 °C. The cells were then collected and analyzed, using flow cytometer (Gallios BD, Beckman Coulter; Tokyo, Japan). Data was analyzed by Kaluza Analysis Software (Beckman Coulter).

2.12. Annexin V-FITC/PI staining

Cells pre-treated with CA9 inhibitors were stained with Annexin V-FITC/PI kit (Sigma Aldrich, APOF-20TST) according to the manufacturer's instructions. The stained cells were diluted by binding buffer and suspended. Flow cytometry (Gallios BD, Beckman Coulter) was used to analyze staining intensity.

2.13. Transmission electron microscopy

MM cells pre-treated with CA9 inhibitor (S4) was fixed with 2 mM glutaraldehyde in 1 mM PBS as previously described [47]. Transmission electron microscopy was performed with a JEM-1400PLUS (JEOL; Tokyo, Japan).

2.14. siRNA transfection

Cells (5×10^4) were seeded in 6-well plate and cultured in normoxia for 16 h. Two silencer select *si*RNAs to human CA9 (Invitrogen; s2270 and s224790) and one negative control *si*RNA (Invitrogen; 4390844) were used. *si*RNA complexes were generated by the use of RNAiMAX (Invitrogen; 13778) transfection reagent in Opti-MEM (Gibco; A4124801), followed by incubation at RT for 15 min. RNA and protein were extracted after *si*RNA treatment for 48 or 72 h under hypoxia.

2.15. Analysis of mitochondria morphology

Cells treated with CA9 inhibitor (S4) were stained with MitoTracker Red for 30 min in normoxia. Cells were fixed with 4% (w/v) paraformaldehyde for 10 min at RT, followed by incubation with ice-cold acetone for 5 min. Images were captured with a confocal microscope (LSM880, Carl Zeiss) and mitochondrial morphology was analyzed by FIJI distribution of ImageJ platform (MiNA) according to the instructions [48].

2.16. Statistics

All statistical analyses were performed with GraphPad Prism 5 software (GraphPad Software, La Jolla, CA). Significance of difference was determined by unpaired *t*-test, one-way *ANOVA* or two-way

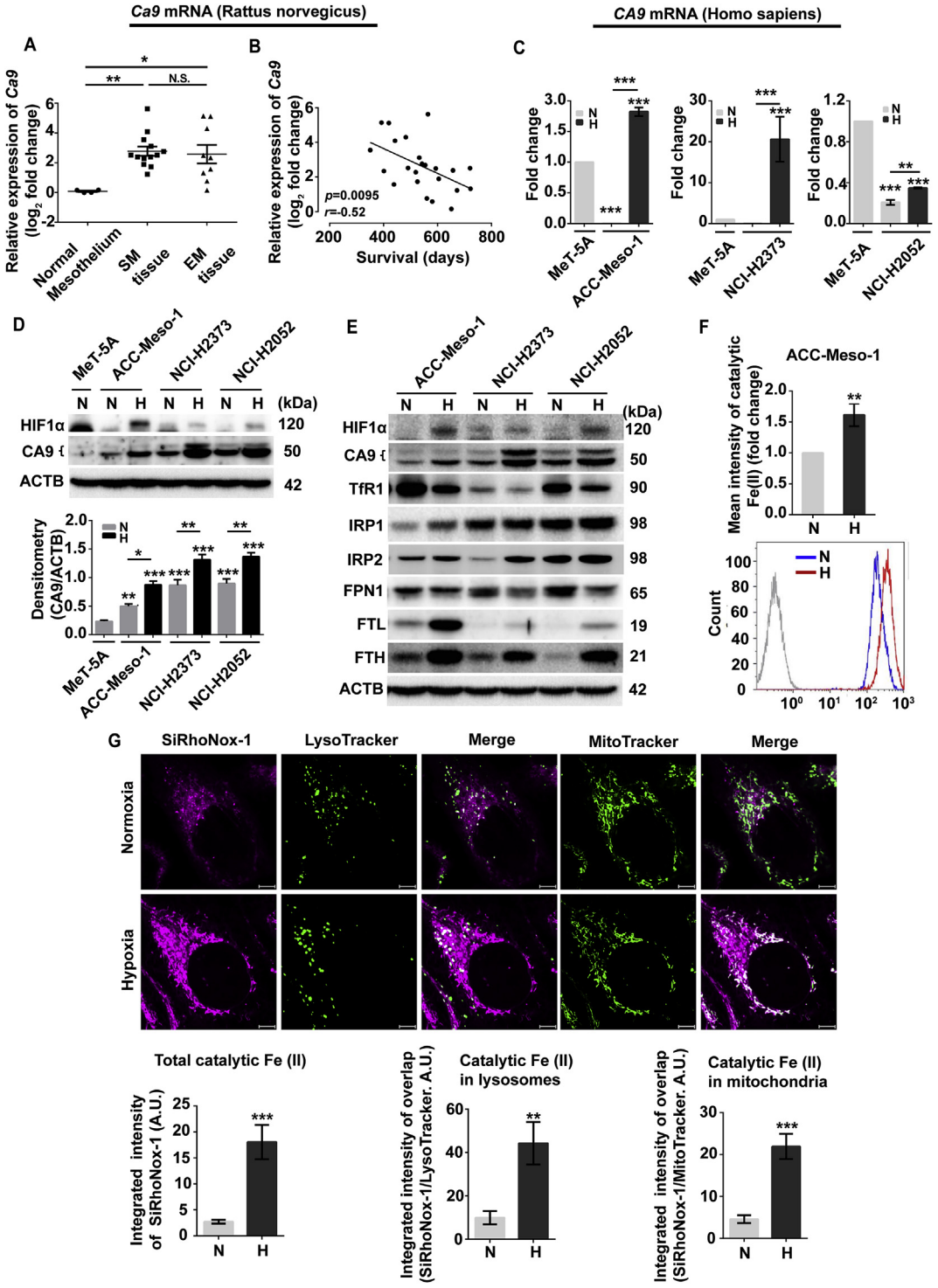

Fig. 1. CA9 overexpression in MM cells correlates with increased catalytic Fe(II) in response to hypoxia. (A) Differential overexpression of *Ca(r)9* in asbestos-induced rat MM previously analyzed by expression array. Normal mesothelium (N = 2)/Met-5A cells (N = 2) in combination (N = 4) were used as a control; SM (N = 13) or EM (N = 9) represent sarcomatoid or epithelioid subtypes of malignant mesothelioma (MM) [6,49]. **(B)** *Ca(r)9* overexpression in MM samples (shown in **A** plus biphasic subtype; N = 2; total N = 24) exhibited an inverse correlation with rat survival [6]. Pearson's correlation coefficient and corresponding P value is indicated. Quantitative RT-PCR **(C)** using *GAPDH* and western blotting **(D)** using β-actin, as corresponding internal standards, were performed to access *CA9* mRNA and protein levels by using two human EM (ACC-Meso-1 and NCI–H2052) and one SM (NCI–H2373) cell lines in comparison to non-tumorous human mesothelial cell (MeT-5A) after 48 h-incubation in normoxia (N) or hypoxia (H; 1% O_2). **(E)** Western blotting was performed to determine levels of iron metabolism-associated proteins in MM cells after 48 h-incubation in normoxia or hypoxia. **(F)** Differential levels of catalytic Fe(II) in normoxia or hypoxia of ACC-Meso-1 cells were determined by staining with SiRhoNox-1 (5 μM), followed by evaluation with a flow cytometer after 48 h-incubation. **(G)** Localization of catalytic Fe(II) in normoxic or hypoxic ACC-Meso-1 cells were analyzed by co-staining of SiRhoNox-1 (5 μM), LysoTracker (200 μM) and MitoTracker (75 μM) after 48 h-incubation and observation with a confocal microscope. Integrated intensity per cell (N = *7*) was quantified by ZEN Imaging Software (ZEISS) (means ± SEM; $*P < 0.05$, $**P < 0.01$, $***P < 0.001$ *vs* each control unless indicated by bar). Refer to text for details. SM, sarcomatoid mesothelioma; EM, epithelioid mesothelioma; N, normoxia; H, hypoxia; A.U., arbitrary unit.

ANOVA, followed by *Turkey*'s multiple comparison test. Significance was defined as $P < 0.05$.

3. Results

3.1. Hypoxia promotes CA9 overexpression in MM cells with increased intracellular catalytic Fe(II)

We previously generated asbestos-induced rat MMs and analyzed them with expression microarray (GEO Accession No. GSE48298) [49]. Here re-analysis revealed that *Ca9* was most highly expressed among all the CAs on the chip (*Ca1, 7, 8, 9, 11, 12* and *15*) in sarcomatoid subtype MM in comparison to epithelioid subtype, and was still significantly overexpressed in both the subtypes of MM ($P < 0.01$ and $P < 0.05$, respectively; Fig. 1A). Furthermore, *Ca9* overexpression in MM, including all the three subtypes (epithelioid, biphasic and sarcomatoid subtypes), showed an inverse correlation (Pearson's correlation, $r = -0.52$, $P = 0.0095$) with survival (Fig. 1B). Thus, we decided to study *Ca9*. For further study, we selected two epithelioid (ACC-Meso-1 and NCI–H2052) and one sarcomatoid (NCI–H2373) human MM cell lines, together with one immortalized mesothelial cell line (MeT-5A).

Because *CA9* is among highly expressed genes in response to hypoxia [35,50] and previous reports demonstrated that most solid tumors display low oxygen level (< 1.3% O_2) [51], we evaluated *CA9* expression by exposing MM cells in both hypoxic (1% O_2 and 5% CO_2 in N_2 balanced atmosphere) and normal (5% CO_2) culture conditions. Incubations were up to 48 h because MM cell proliferation under the two conditions revealed no significant difference within such periods (Fig. S1A). ACC-Meso-1 ($P < 0.001$) and NCI–H2373 ($P < 0.001$), but not NCI–H2052, cultured under hypoxia displayed higher levels of *CA9* mRNA in comparison to MeT-5A cultured in normoxia, considering that normal mesothelium is exposed to physiological level of O_2 (Fig. 1C). CA9 protein levels were significantly ($P < 0.05$ or $P < 0.01$) increased in all the three MM cell lines in response to hypoxia and all MM cell lines exhibited higher CA9 protein levels compared with Met-5A (Fig. 1D).

We found high expression of HIF-1α in MeT-5A in normoxia (Fig. 1D), which might be the reason of increased *CA9* mRNA in MeT-5A in normoxia in comparison to MM cells (Fig. 1C). However, CA9 protein level in MeT-5A did not show a significant ($P = 0.11$) increase in response to hypoxia (Fig. S1C). We then evaluated the expression levels of iron metabolism-associated proteins in MM cells in response to hypoxia. The results exhibited decreased protein levels of iron transporters, TFRC and FPN-1(SLC40A1) with increased iron storage proteins, FTL and FTH (Fig. 1E). Further, IRP2 proteins increased in response to hypoxia with time-dependence (Fig. S1B), consistent with previous studies that hypoxia promotes up-regulation of IRP2 with a posttranslational mechanism involving protein stability [29]. Of note, a significantly ($P < 0.01$) elevated catalytic Fe(II) signals were detected (Fig. 1F), a portion of which were co-localized both with lysosomes ($P < 0.01$) and mitochondria ($P < 0.001$) (Fig. 1G) in ACC-Meso-1 cells in response to hypoxia.

3.2. CA9-specific inhibitors delay proliferation and block migration of MM cells under hypoxia

To study the significance of CA9 expression in MM cells, we treated ACC-Meso-1 cells under hypoxia with two distinct CA9-specific inhibitors, U104 [52] and S4 [53]. S4 or U104 treatment significantly ($P < 0.001$; both S4 and U104) decreased cell viability of ACC-Meso-1 cells at 48 and 72 h post treatment whereas vehicle treatment (DMSO) showed no effect on proliferation (Fig. 2A). Both S4 and U104 revealed antiproliferative effects ($P < 0.001$ and $P < 0.01$, respectively) on Met-5A cells though the effects were milder than in ACC-Meso-1 cells (Fig. 2B). As previous studies indicated a linkage between *CA9* overexpression and metastasis in various cancers [54], we then evaluated the effect of CA9 inhibition on MM cell migration with wound healing assay. In contrast to vehicle treatment, S4 or U104 treatment under hypoxia dose-dependently (40 and 75 μM) reduced migration of ACC-Meso-1 cells at 24 h (Fig. 2C). These results suggest that CA9 activity is essential for MM cells to proliferate and migrate.

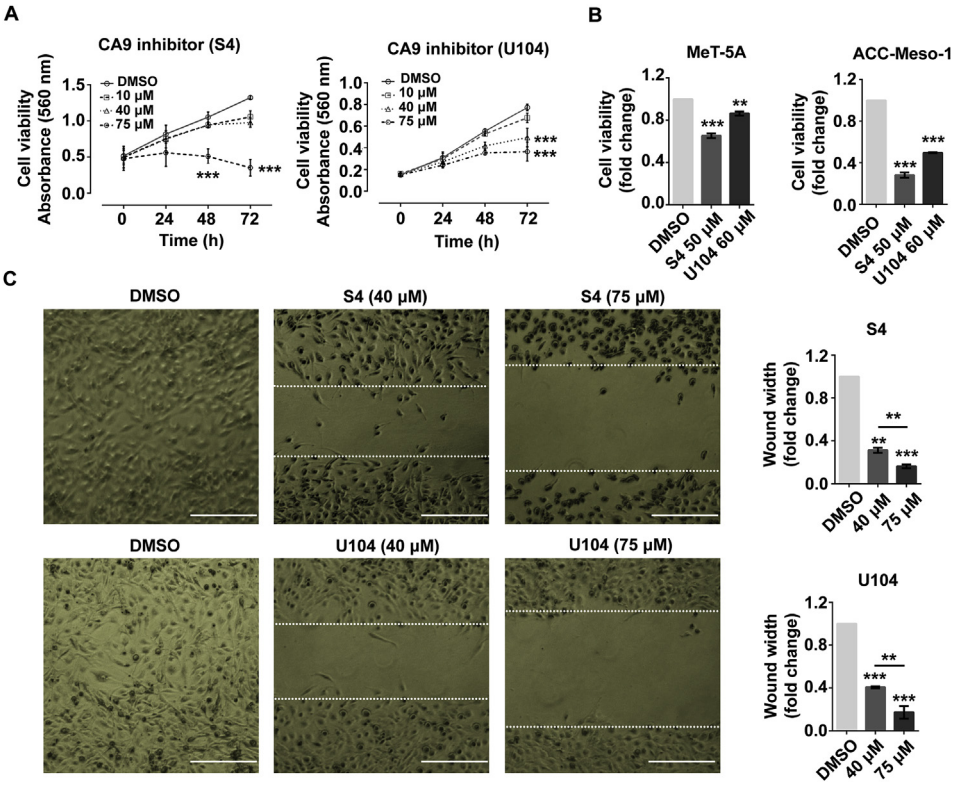

Fig. 2. CA9 inhibition antagonizes MM cell growth and migration under hypoxia. ACC-Meso-1 and MeT-5A cells were cultured under hypoxia and treated with two CA9 inhibitors (S4 and U104). MTT **(A)** or WST-1 **(B)** assay was performed to evaluate anti-proliferation effect resulted from CA9 inhibitors in ACC-Meso-1 cells. MeT-5A was used as a non-tumorous control to evaluate the cytotoxic effect caused by CA9 inhibitors. **(C)** Wound healing assay was performed to estimate migration ability of ACC-Meso-1 cells in response to CA9 inhibition. Cell migration was evaluated by measurement of wound closure prior to (0 h) and after incubation with CA9 inhibitors (24 h). DMSO (0.5% v/v) as a vehicle was used as a negative control (scale bar = 100 μm; means ± SEM; $*P < 0.05$, $**P < 0.01$, $***P < 0.001$ *vs* control [DMSO vehicle] unless indicated by bar). Refer to text for details.

3.3. CA9 inhibition under hypoxia results in iron overload in lysosomes and mitochondria, inducing oxidative stress and triggering lipid peroxidation in MM cells

To study whether CA9 is associated with iron metabolism in MM cells under hypoxia, we evaluated the expression levels of iron-associated proteins after CA9 inhibition in MM cells under hypoxia. S4 or U104 treatment in ACC-Meso-1 cells showed a dose-dependent decrease in CA9 expression under hypoxia. The protein levels of TFRC and FPN-1 were increased whereas those of FTL and FTH were decreased, consistent with up-regulation of iron-regulatory proteins, IRP1 and IRP2. (Figs. 3A and S2A).

Notably, these alterations were similar to the previous findings that abundant intracellular iron contributes to ferroptosis, a recently defined regulated necrosis dependent on catalytic Fe(II), through increasing iron-uptake (TFRC) and decreasing iron storage (FTL/H) [55,56] and/or with NCOA4-mediated ferritin autophagy (ferritinophagy) [57]. Thus, we decided to determine levels and localization of catalytic Fe(II) in response to CA9 inhibition. S4 or U104 treatment in ACC-Meso-1 cells significantly increased the level of catalytic Fe(II) ($P < 0.01$ and $P < 0.05$, S4 and U104, respectively) (Fig. 3B), which was accompanied by oxidative stress (peroxides and mitochondrial O_2^-) and lipid peroxidation (Fig. 3C, D, 3E), surrogate markers for ferroptosis [56,58]. We also performed *si*RNA-induced *CA9* knockdown in ACC-Meso-1 cells under hypoxia. Transfection of *si*RNA (20 nM) exhibited similar effects on the levels of iron metabolism-associated proteins as well as increased catalytic Fe(II) and lipid peroxidation (Figs. S2B, S2C, S2D). We then analyzed the distribution of catalytic Fe(II) with a confocal microscopy, which disclosed that overall catalytic Fe(II) signals were significantly increased with more localization in lysosomes (LysoTracker) and in mitochondria (MitoTracker) ($P < 0.001$; N = 20) (Fig. 3F). These results suggest that CA9 plays a role in maintaining iron homeostasis in hypoxic MM cells.

3.4. CA9 inhibition under hypoxia leads to mitochondrial fission, contributing to autophagy in MM cells

Simultaneously with iron excess in mitochondria and lysosomes, we observed abnormality in mitochondrial morphology, displaying an increase in fragmented structure in response to S4 treatment (75 μM) in ACC-Meso-1 cells cultured under hypoxia (Figs. 3F and 4A). We measured the length of each mitochondrion stained with MitoTracker. S4-treated ACC-Meso-1 cells under hypoxia exhibited shortened ($P < 0.001$) mitochondrial length compared with the control group

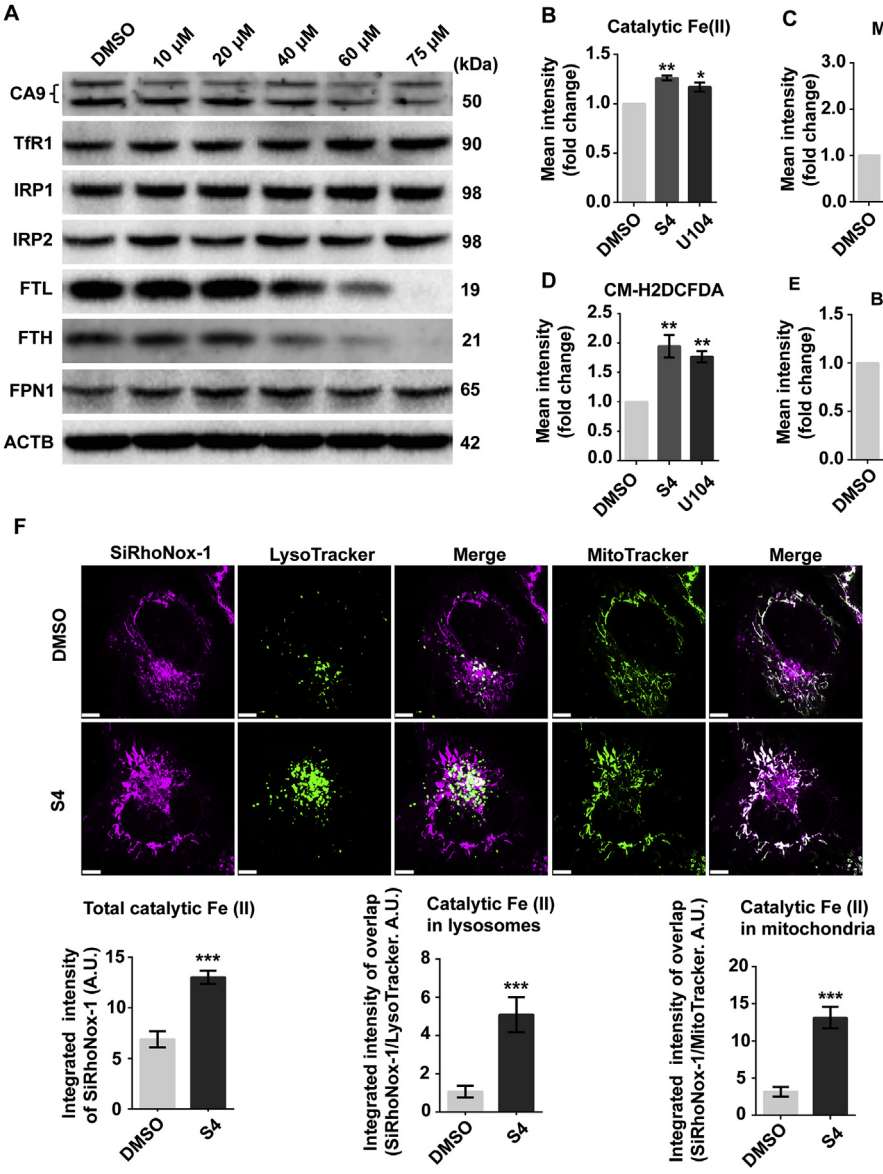

Fig. 3. CA9 inhibition under hypoxia augments increase in catalytic Fe(II) with oxidative stress in mitochondria and lysosomes in MM cells. (A) Protein levels of CA9 and iron metabolism-associated proteins in ACC-Meso-1 cells after 48 h S4 treatment under hypoxia. **(B)** Levels of catalytic Fe(II) (SiRhoNox-1, 5 μM); **(C)** generation of mitochondrial O_2^- (MitoSox, 5 μM); **(D)** total cellular peroxides (CM-H2DCFDA, 5 μM) and **(E)** total lipid peroxidation (BODIPY, 2 μM) were quantified with FACS in response to S4 or U104 treatment (75 μM) under hypoxia for 48 h. **(F)** Localization of catalytic Fe(II) in S4-treated (75 μM) ACC-Meso-1 cells were determined by co-staining of SiRhoNox-1 (5 μM), LysoTracker (200 nM) and MitoTracker (75 nM) together after 48 h-hypoxic culture, followed by observation with a confocal microscope. DMSO as vehicle was used as negative control (0.5% v/v). Scale bar = 5 μm (N = 20; means ± SEM. $^*P < 0.05$, $^{**}P < 0.01$, $^{***}P < 0.001$ *vs* control [DMSO vehicle]). Refer to text for details.

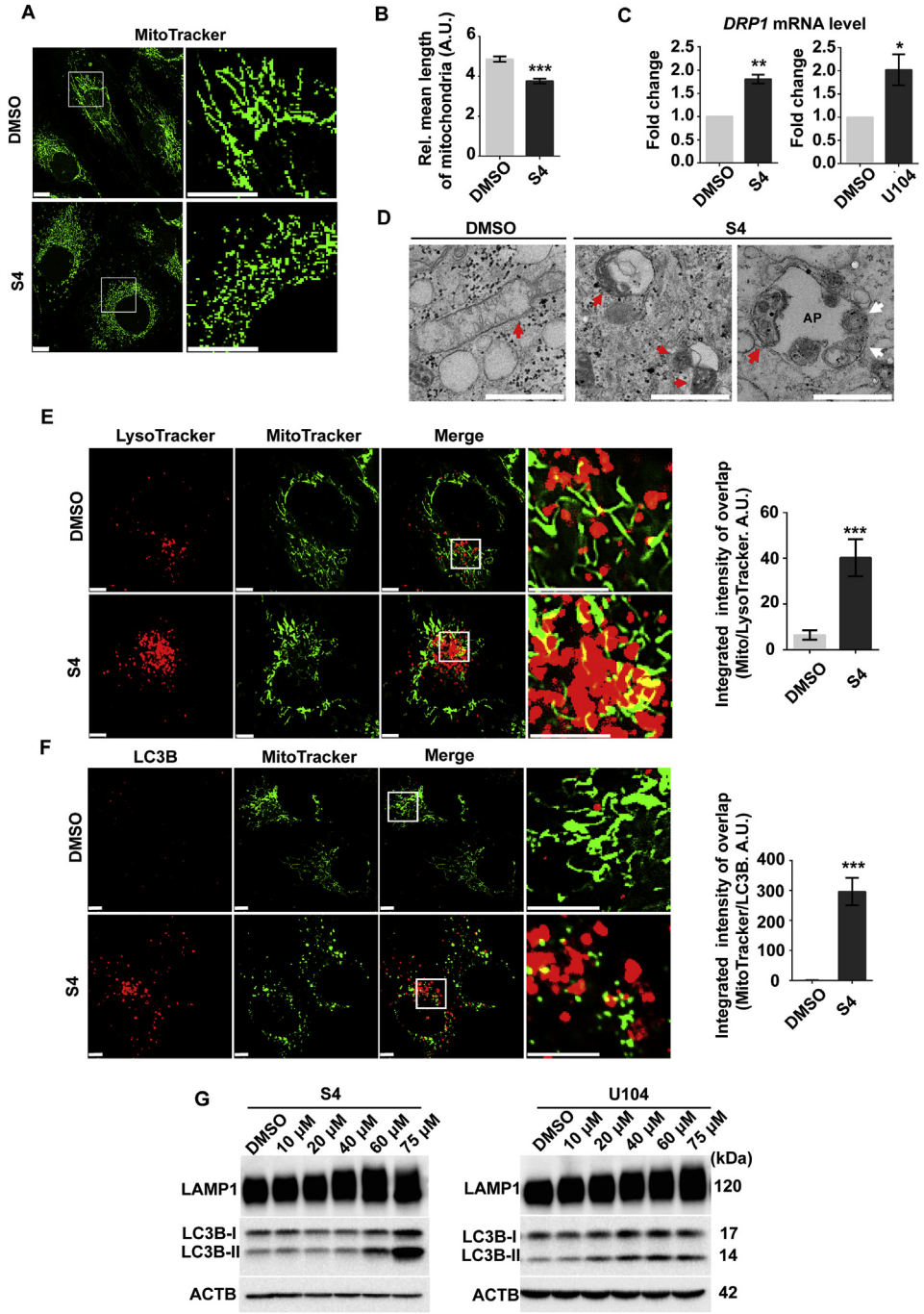

Fig. 4. CA9 inhibition induces mitochondrial fission and mitophagy in MM cells under hypoxia. (A) After treatment with S4 (75 μM) under hypoxia for 48 h, ACC-Meso-1 cells were stained by MitoTracker (200 nM) for 30 min, then fixed by 4% paraformaldehyde (PFA). Mitochondrial morphology was observed with a confocal microscope (scale bar = 10 μm). **(B)** The length of mitochondria was quantified with an ImageJ software (N = 20). Rel, relative. **(C)** Quantitative RT-PCR was performed to evaluate *DRP1* mRNA level after treatment with S4 or U104 (40 μM) for 48 h under hypoxia by using *GAPDH* as internal standard. **(D)** Electron transmission microscope was used to examine the mitochondrial morphology after S4 treatment (75 μM) in ACC-Meso-1 cells for 48 h under hypoxia (bar = 1 μm). Red or white arrows represent mitochondrion or lysosome, respectively; AP represents autophagosome. **(E)** The same samples (shown in Fig. 3E) were used to demonstrate mitophagy, identified by co-staining of LysoTracker and MitoTracker in S4-treated (75 μM) ACC-Meso-1 cells (N = 20). **(F)** Immunofluorescent analyses were performed to confirm mitophagy. Cells were incubated with LC3 antibody (1:1000), following MitoTracker (200 nM) staining and fixation by 4% PFA (N = 10; scale bar = 5 μm). **(G)** Expression of LC3 and LAMP1 was evaluated in ACC-Meso-1 cells after treatment with S4 or U104 for 48 h under hypoxia (means ± SEM; $^{*}P < 0.05$, $^{**}P < 0.01$, $^{***}P < 0.001$ *vs* control [DMSO vehicle]). Refer to text for details. (For interpretation of the references to colour in this figure legend, the reader is referred to the Web version of this article.)

(Fig. 4B). We also found increased ($P < 0.01$ and $P < 0.05$; S4 and U104, respectively) transcription of *DRP1*, encoding dynamin-related protein to catalyze the mitochondrial fission [59], after S4 (40 μM) or U104 (75 μM) treatment under hypoxia for 48 h (Fig. 4C). To further confirm this, we performed transmission electron microscopy. S4-treated ACC-Meso-1 cells presented diverse abnormities in mitochondria, showing swelling, membrane rupture and fragmentation as well as engulfment by autophagic vacuoles (mitophagy) (Fig. 4D). A significant ($P < 0.001$) increase in merged staining area (yellow) of Mito and LysoTracker was detected in S4-treated ACC-Meso-1 cells, which was rare in untreated control group under hypoxia for 48 h (Fig. 4E). Further confirmation of mitophagy was achieved by immunofluorescence staining of LC3B, a marker of autophagosome, and MitoTracker. S4-treated ACC-Meso-1 cells displayed a significantly ($P < 0.001$) increased LC3B and MitoTracker merge staining (yellow) (Fig. 4F). In addition to LC3B, we also examined the protein level of LAMP-1, a marker for autophagosome and lysosome, by immunoblotting. Increased expression of both LAMP-1 and LC3B-II (lipidated form) were observed in a dose-dependent manner in response to S4 or U104 treatment in ACC-Meso-1 cells under hypoxia for 48 h (Fig. 4G).

3.5. CA9 inhibition induces both apoptosis and ferroptosis

S4 or U104 (75 μM) caused significant cell death detected by SYTOX Green at 48 h in ACC-Meso-1 cells under hypoxia (Fig. 5A). To define the mode of cell death induced by CA9 inhibition in MM cells, we first evaluated apoptotic markers. Both S4 and U104-treated ACC-Meso-1 cells showed a significant ($P < 0.05$ and $P < 0.01$; S4 and U104, respectively) increase in late apoptotic cells (Annexin V-FITC^{+}/PI^{+}; shown as B+/+) under hypoxia (Fig. 5B). U104-treated MM cells also

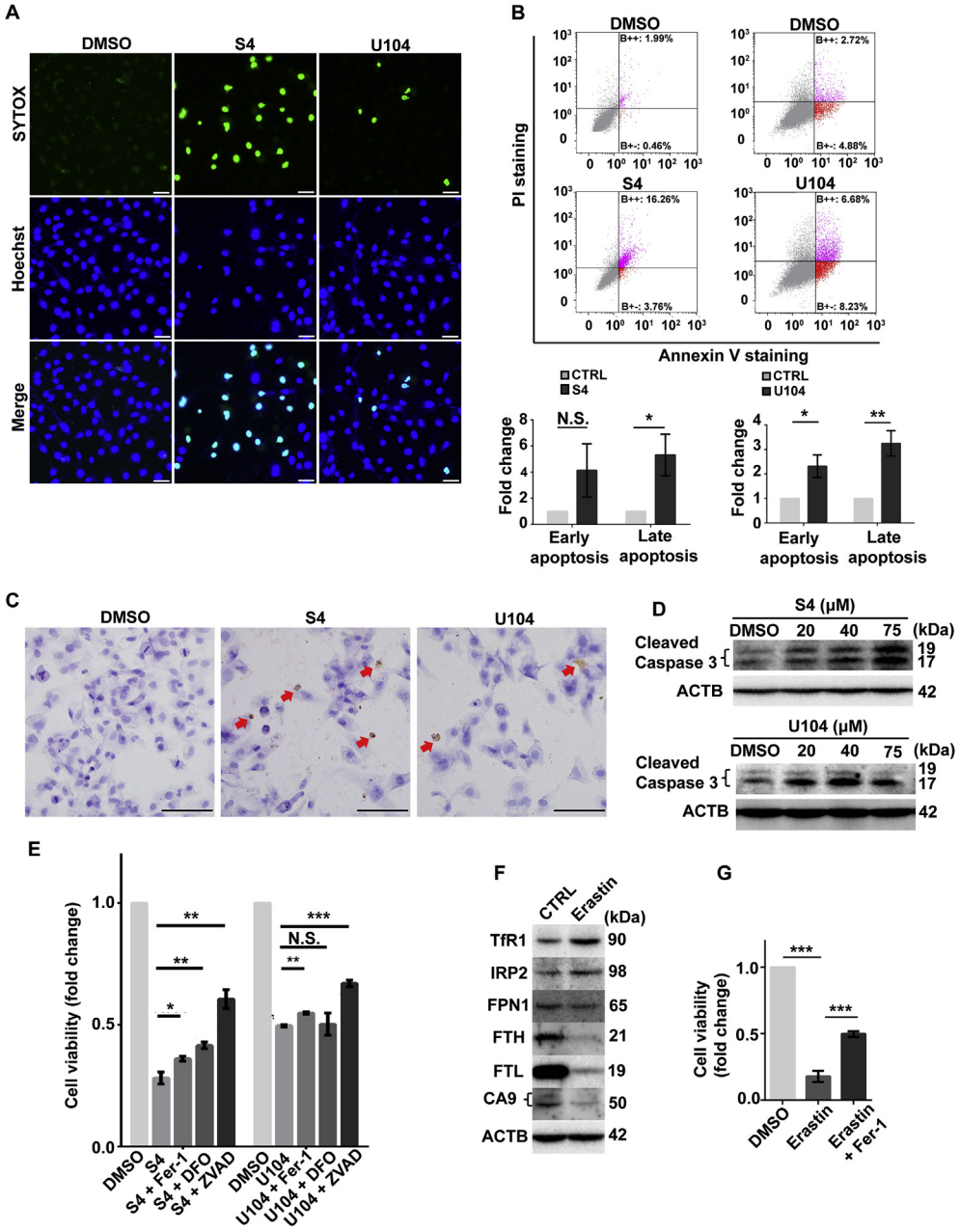

Fig. 5. CA9 inhibition under hypoxia induced both apoptosis and ferroptosis in MM cells. (A) SYTOX Green staining of ACC-Meso-1 cells was performed to evaluate the effects of CA9 inhibitors (S4 and U104, 75 μM), which induced regulated cell death after 48 h-incubation under hypoxia (scale bar = 50 μm). Apoptosis was determined by detection of FITC-Annexin V with FACS **(B)** and TUNEL assay **(C)**. **(D)** Expression of cleaved caspase-3 in ACC-Meso-1 cells was accessed by western blotting after 48 h-treatment with S4 or U104 under hypoxia. **(E)** Effects of Fer-1 (3 μM), DFO (0.5 μM) and Z-VAD (50 μM) on S4 and U104 induced cell death (S4 50 μM or U104 60 μM) were evaluated after 72 h-treatment under hypoxia. **(F)** Effect of erastin (20 μM) on CA9 and iron metabolism-associated proteins and cell viability **(G)** in hypoxic ACC-Meso-1 cell (means ± SEM; $^{*}P < 0.05$, $^{**}P < 0.01$, $^{***}P < 0.001$ *vs* each control (CTRL) unless indicated by bar). Refer to text for details. (For interpretation of the references to colour in this figure legend, the reader is referred to the Web version of this article.)

revealed a significant ($P < 0.05$) increase in early apoptotic cells (Annexin V-FITC^{+}/PI^{-}, shown as B+/-) whereas S4 did not. Confirmation of apoptosis was performed with TUNEL assay and validation of protein levels of cleaved caspase-3. Treatment with S4 or U104 (75 μM) not only induced TUNEL-positive cells with nuclear fragmentation but also increase in cleaved caspase-3 in ACC-Meso-1 cells cultured under hypoxia (Fig. 5C and D).

Because we observed increased catalytic Fe(II) with oxidative stress and lipid peroxidation (Fig. 3C–E) as well as mitophagy (Fig. 4EG) after CA9 suppression in MM cells, we speculated the involvement of ferroptosis. To study the association of ferroptosis, ferroptotic (Fer-1) and apoptotic (Z-VAD) inhibitors as well as an iron chelator (DFO) were co-treated with S4 or U104 in ACC-Meso-1 cells under hypoxia. Z-VAD (50 μM) treatment significantly ($P < 0.01$ and $P < 0.001$, respectively) reversed CA9 inhibition-induced cell death by S4 (50 μM) or U104 (60 μM) treatment at 72 h (Fig. 5E). Fer-1 (3 μM) was significantly effective against S4 and U104 treatment ($P < 0.05$ and $P < 0.01$, respectively). DFO at a low concentration (0.5 μM) significantly ($P < 0.01$) attenuated S4-induced cytotoxic effect. Furthermore, we evaluated ferroptosis induced by a classical inducer, erastin, in ACC-Meso-1 cells and compared the levels of iron metabolism-associated proteins between those of CA9 inhibitors and of erastin. Erastin (20 μM)-induced MM cell death under hypoxia ($P < 0.001$) was reversed ($P < 0.001$) by Fer-1 (3 μM) at 48 h (Fig. 5G). Furthermore, a similar expression patterns of iron metabolism-associated proteins were recognized when compared with CA9 inhibitor treatment, such as increased TFRC, IRP2 and decreased FTH/L. Of note, CA9 protein level was decreased after erastin treatment, suggesting the involvement of CA9 in erastin-induced ferroptosis (Figs. 5F and 3A). Thus, MM cell death induced by CA inhibition revealed the characteristics of both apoptosis and ferroptosis.

4. Discussion

Excess iron has been associated with carcinogenesis through Fenton reaction catalyzed by Fe(II) [8,10,60]. Cancer may originate as side

effects of using iron and oxygen for a long time [7,61]. Carbonic anhydrases (*CA*s; EC 4.2.1.1) are a superfamily (CA1-16) of metalloenzymes, equilibrating the reactions among CO_2, bicarbonate and H^+ [32], and thus are indispensable for intracellular pH regulation. Carbonic anhydrase 9 (CA9), a membrane-associated α-CA, has recently been a prognosis marker and also a drug target for various cancers [33]. In the present study we for the first time showed an intimate association of iron metabolism with hypoxia and redox regulation, where CA9 plays a central role at least in MM tumor cells, an iron excess-associated cancer [6]. Of note, this association was not observed in non-tumorous mesothelial cells (MeT-5A). Therefore, CA9 is an appropriate molecular target for the therapy of MM.

Cancer is now recognized as a disease of the genome, in which each cancer has its own evolutionary process through distinct mutation burdens [62]. Cancer presents characteristics of persistent proliferation (DNA replication and mitosis) and invasion, sometimes metastasis. Indeed, this is not easy, considering the coexistent hypoxia inside when the tumor becomes large with relative deficiency in vasculature and simultaneous need for abundant iron for DNA replication, starting with ribonucleotide reductase where iron is a cofactor [63]. Here we suggest, based on our results, that CA9 overexpression via HIF-1α activation works as a magic bullet for cancer: 1) CO_2 elimination with regulation of intracellular pH for better cellular metabolism; 2) higher intracellular pH reduces soluble iron, including catalytic Fe(II) [60]; 3) hypoxia and extracellular acidity provide tumor microenvironment for selection over other kinds of non-tumorous cells under evolutionary pressure and proliferation [2], which may be efficiently performed at the outer plasma membrane by CA9. We have to be reminded that the first life on earth was born in the ancient sea of full of catalytic Fe(II), thus in a low pH [64]. In the present study we demonstrated that CA9 inhibition by specific inhibitors or by knocking down under hypoxia obstructs cellular proliferation and migration of MM, eventually leading to MM cell death.

Recently, fluorescent turn-on probes for catalytic Fe(II) have become available for time-lapse cell culture study or for frozen sections [46,65–67], which provides precious information *in situ*. By the use of these probes, we found that catalytic Fe(II) is significantly increased with hypoxia in lysosomes, mitochondria and cytosol (Fig. S3A), which was further promoted by CA9 inhibition with enhancement in lysosomes and mitochondria (Fig. S3B). Interestingly, the alterations in expression of iron metabolism-associated genes were opposite in MM cells between hypoxia only and CA9 inhibition under hypoxia. Namely, hypoxia alone condition caused a logical response in iron metabolism to increased catalytic Fe(II) in MM cells. Namely, iron increment, presumably caused by increased solubility of iron according with the lowered pH, resulted in low iron intake and high iron storage to prevent iron toxicity. The results may be associated with the fact that efficiency of iron transporters, such as ZIP8/14 (SLC39A14) [68] and SLC11A2 [69], are pH-dependent. Still the MM cells tried to reserve iron intracellularly by decreasing FPN-1 [70].

However, in the case of CA9 inhibition with simultaneous hypoxia, MM cells responded to a situation of further increase in catalytic Fe(II) as if they lack iron, requiring more (seeking high iron intake and low storage with tight regulation). This is presumably due to a lethal condition, including critically increased lysosomal and mitochondrial catalytic Fe(II), resulting in oxidative stress and lipid peroxidation. Whereas how iron is transported across the mitochondrial outer membrane is not elucidated yet, the results indicate that CA9 at least partially controls iron metabolism in cells. Here the MM cells tried to purge catalytic Fe(II) outside by increased FPN-1. Autophagy can promote iron availability for tumor survival under hypoxia [71] and we believe that this mechanism was in motion. We observed on this condition numerous mitochondrial abnormalities, including fission, disruption and mitochondrial autophagy (mitophagy), consistent with other conditions involving oxidative stress or iron excess [72,73]. Based on the results, we further analyzed the modes of MM cell death after CA9 inhibition under hypoxia, and found that this is a mixed cell death of apoptosis and ferroptosis [56] through autophagic process. Currently, there are twelve distinct modes of regulated cell death defined [74]. We recognized that three distinct modes of regulated cell death (autophagy, ferroptosis and apoptosis) were involved in the case of MM cell death by CA9 inhibition under hypoxia.

Limitations of our present work are: 1) specificities of the CA9 inhibitors are not complete [34], so we also performed knockdown experiments to confirm the results; 2) MM cells most probably evolved under excess iron environment during carcinogenesis [7], so further studies on other kinds of cancer are warranted to confirm that our results are universal for cancer.

In conclusion, CA9 plays a pivotal role in the metabolism of MM cells under hypoxia, providing numerous merits, such as proliferation and migration, where iron homeostasis is maintained for their optimal growth with minimal oxidative cytotoxicity to avoid ferroptosis and apoptosis. Therefore, CA9 is an attractive molecular target for chemotherapy of MM, considering the present dismal therapeutic status [15]. Because CAs have been a drug target for various pathologies, including cancers, glaucoma, obesity and Alzheimer's disease [34,75], reexploration of other pathologies from the viewpoint of catalytic Fe(II) might be fruitful.

Conflicts of interest

The authors have no conflicts of interests to disclose.

Acknowledgements

This work was supported, in part, by a Japan Society for the Promotion of Science (JSPS) Kakenhi (JP17H04064 and JP19H05462) and Private University Research Branding Project to Shinya Toyokuni (ST).

Appendix A. Supplementary data

Supplementary data to this article can be found online at https://doi.org/10.1016/j.redox.2019.101297.

References

[1] F. Bray, J. Ferlay, I. Soerjomataram, R.L. Siegel, L.A. Torre, A. Jemal, Global cancer statistics 2018: GLOBOCAN estimates of incidence and mortality worldwide for 36 cancers in 185 countries, CA A Cancer J. Clin. 68 (6) (2018) 394–424.
[2] M. Logozzi, C. Capasso, R. Di Raimo, S. Del Prete, D. Mizzoni, M. Falchi, C.T. Supuran, S. Fais, Prostate cancer cells and exosomes in acidic condition show increased carbonic anhydrase IX expression and activity, J. Enzym. Inhib. Med. Chem. 34 (1) (2019) 272–278.
[3] B. Robinson, R. Lake, Advances in malignant mesothelioma, N. Engl. J. Med. 353 (15) (2005) 1591–1603.
[4] S.H. Chew, S. Toyokuni, Malignant mesothelioma as an oxidative stress-induced cancer: an update, Free Radic. Biol. Med. 86 (2015) 166–178.
[5] A.F. Gualtieri, G.B. Andreozzi, M. Tomatis, F. Turci, Iron from a geochemical viewpoint. Understanding toxicity/pathogenicity mechanisms in iron-bearing minerals with a special attention to mineral fibers, Free Radic. Biol. Med. 133 (2019) 21–37.
[6] L. Jiang, S. Akatsuka, H. Nagai, S.H. Chew, H. Ohara, Y. Okazaki, Y. Yamashita, Y. Yoshikawa, H. Yasui, K. Ikuta, K. Sasaki, Y. Kohgo, S. Hirano, Y. Shinohara, N. Kohyama, T. Takahashi, S. Toyokuni, Iron overload signature in chrysotile-induced malignant mesothelioma, J. Pathol. 228 (2012) 366–377.
[7] S. Toyokuni, Iron addiction with ferroptosis-resistance in asbestos-induced mesothelial carcinogenesis: toward the era of mesothelioma prevention, Free Radic. Biol. Med. 133 (2019) 206–215.
[8] S. Toyokuni, Role of iron in carcinogenesis: cancer as a ferrotoxic disease, Cancer Sci. 100 (1) (2009) 9–16.
[9] H. Nagai, T. Ishihara, W.H. Lee, H. Ohara, Y. Okazaki, K. Okawa, S. Toyokuni, Asbestos surface provides a niche for oxidative modification, Cancer Sci. 102 (2011) 2118–2125.
[10] S. Toyokuni, F. Ito, K. Yamashita, Y. Okazaki, S. Akatsuka, Iron and thiol redox signaling in cancer: an exquisite balance to escape ferroptosis, Free Radic. Biol. Med. 108 (2017) 610–626.
[11] S. Toyokuni, Mechanisms of asbestos-induced carcinogenesis, Nagoya J. Med. Sci. 71 (1–2) (2009) 1–10.

[12] Y. Ohara, S.H. Chew, T. Shibata, Y. Okazaki, K. Yamashita, S. Toyokuni, Phlebotomy as a preventive measure for crocidolite-induced mesothelioma in male rats, Cancer Sci. 109 (2) (2018) 330–339.

[13] H. Nagai, Y. Okazaki, S.H. Chew, N. Misawa, H. Yasui, S. Toyokuni, Deferasirox induces mesenchymal-epithelial transition in crocidolite-induced mesothelial carcinogenesis in rats, Cancer Prev. Res. 6 (2013) 1222–1230.

[14] L. Jiang, S.H. Chew, K. Nakamura, Y. Ohara, S. Akatsuka, S. Toyokuni, Dual preventive benefits of iron elimination by desferal in asbestos-induced mesothelial carcinogenesis, Cancer Sci. 107 (7) (2016) 908–915.

[15] A. Scherpereel, F. Wallyn, S.M. Albelda, C. Munck, Novel therapies for malignant pleural mesothelioma, Lancet Oncol. 19 (3) (2018) e161–e172.

[16] S. Renvall, J. Niinikoski, Kinetics of oxygen in peritoneal cavity. Effects of chemical peritonitis and intraperitoneally administered colloids in rats, J. Surg. Res. 28 (2) (1980) 132–139.

[17] R.J. Francis, T. Segard, L. Morandeau, Y.C. Lee, M.J. Millward, A. Segal, A.K. Nowak, Characterization of hypoxia in malignant pleural mesothelioma with FMISO PET-CT, Lung Cancer 90 (1) (2015) 55–60.

[18] N. Nabavi, K.L. Bennewith, A. Churg, Y. Wang, C.C. Collins, L. Mutti, Switching off malignant mesothelioma: exploiting the hypoxic microenvironment, Genes Cancer 7 (11–12) (2016) 340–354.

[19] M.C. Kim, S.H. Hwang, N.Y. Kim, H.S. Lee, S. Ji, Y. Yang, Y. Kim, Hypoxia promotes acquisition of aggressive phenotypes in human malignant mesothelioma, BMC Canc. 18 (1) (2018) 819.

[20] A.A. Mujoomdar, T.R. Tilleman, W.G. Richards, R. Bueno, D.J. Sugarbaker, Prevalence of in vitro chemotherapeutic drug resistance in primary malignant pleural mesothelioma: result in a cohort of 203 resection specimens, J. Thorac. Cardiovasc. Surg. 140 (2) (2010) 352–355.

[21] M. Kilic, H. Kasperczyk, S. Fulda, K.M. Debatin, Role of hypoxia inducible factor-1 alpha in modulation of apoptosis resistance, Oncogene 26 (14) (2007) 2027–2038.

[22] S. Fulda, K.M. Debatin, HIF-1-regulated glucose metabolism: a key to apoptosis resistance? Cell Cycle 6 (7) (2007) 790–792.

[23] L. Schito, G.L. Semenza, Hypoxia-inducible factors: master regulators of cancer progression, Trends Cancer 2 (12) (2016) 758–770.

[24] Y.M. Shah, L. Xie, Hypoxia-inducible factors link iron homeostasis and erythropoiesis, Gastroenterology 146 (3) (2014) 630–642.

[25] L. Tacchini, L. Bianchi, A. Bernelli-Zazzera, G. Cairo, Transferrin receptor induction by hypoxia. HIF-1-mediated transcriptional activation and cell-specific post-transcriptional regulation, J. Biol. Chem. 274 (34) (1999) 24142–24146.

[26] Z.M. Qian, X.M. Wu, M. Fan, L. Yang, F. Du, W.H. Yung, Y. Ke, Divalent metal transporter 1 is a hypoxia-inducible gene, J. Cell. Physiol. 226 (6) (2011) 1596–1603.

[27] I. Yanatori, F. Kishi, DMT1 and iron transport, Free Radic. Biol. Med. 133 (2019) 55–63.

[28] B.W. Huang, M. Miyazawa, Y. Tsuji, Distinct regulatory mechanisms of the human ferritin gene by hypoxia and hypoxia mimetic cobalt chloride at the transcriptional and post-transcriptional levels, Cell. Signal. 26 (12) (2014) 2702–2709.

[29] E.S. Hanson, L.M. Foot, E.A. Leibold, Hypoxia post-translationally activates iron-regulatory protein 2, J. Biol. Chem. 274 (8) (1999) 5047–5052.

[30] S.V. Torti, F.M. Torti, Iron and cancer: more ore to be mined, Nat. Rev. Cancer 13 (5) (2013) 342–355.

[31] K.L. Eales, K.E. Hollinshead, D.A. Tennant, Hypoxia and metabolic adaptation of cancer cells, Oncogenesis 5 (2016) e190.

[32] C.T. Supuran, Carbonic Anhydrases and Metabolism, Metabolites 8 (2) (2018) 25.

[33] S. Banerjee, P.A. Deshpande, On origin and evolution of carbonic anhydrase isozymes: a phylogenetic analysis from whole-enzyme to active site, Comput. Biol. Chem. 61 (2016) 121–129.

[34] C.T. Supuran, Carbonic anhydrases: novel therapeutic applications for inhibitors and activators, Nat. Rev. Drug Discov. 7 (2) (2008) 168–181.

[35] C.C. Wykoff, N.J. Beasley, P.H. Watson, K.J. Turner, J. Pastorek, A. Sibtain, G.D. Wilson, H. Turley, K.L. Talks, P.H. Maxwell, C.W. Pugh, P.J. Ratcliffe, A.L. Harris, Hypoxia-inducible expression of tumor-associated carbonic anhydrases, Cancer Res. 60 (24) (2000) 7075–7083.

[36] J. Chiche, K. Ilc, J. Laferriere, E. Trottier, F. Dayan, N.M. Mazure, M.C. Brahimi-Horn, J. Pouyssegur, Hypoxia-inducible carbonic anhydrase IX and XII promote tumor cell growth by counteracting acidosis through the regulation of the intracellular pH, Cancer Res. 69 (1) (2009) 358–368.

[37] M.Y. Mboge, B.P. Mahon, R. McKenna, S.C. Frost, Carbonic anhydrases: role in pH control and cancer, Metabolites 8 (1) (2018) 19.

[38] C. Ryder, K. McColl, F. Zhong, C.W. Distelhorst, Acidosis promotes Bcl-2 family-mediated evasion of apoptosis: involvement of acid-sensing G protein-coupled receptor Gpr65 signaling to Mek/Erk, J. Biol. Chem. 287 (33) (2012) 27863–27875.

[39] M. Swayampakula, P.C. McDonald, M. Vallejo, E. Coyaud, S.C. Chafe, A. Westerback, G. Venkateswaran, J. Shankar, G. Gao, E.M.N. Laurent, Y. Lou, K.L. Bennewith, C.T. Supuran, I.R. Nabi, B. Raught, S. Dedhar, The interactome of metabolic enzyme carbonic anhydrase IX reveals novel roles in tumor cell migration and invadopodia/MMP14-mediated invasion, Oncogene 36 (45) (2017) 6244–6261.

[40] H.J. Shin, S.B. Rho, D.C. Jung, I.O. Han, E.S. Oh, J.Y. Kim, Carbonic anhydrase IX (CA9) modulates tumor-associated cell migration and invasion, J. Cell Sci. 124 (Pt 7) (2011) 1077–1087.

[41] S.C. Chafe, P.C. McDonald, S. Saberi, O. Nemirovsky, G. Venkateswaran, S. Burugu, D. Gao, A. Delaidelli, A.H. Kyle, J.H.E. Baker, J.A. Gillespie, A. Bashashati, A.I. Minchinton, Y. Zhou, S.P. Shah, S. Dedhar, Targeting hypoxia-induced carbonic anhydrase IX enhances immune-checkpoint blockade locally and systemically, Cancer Immunol. Res. 7 (7) (2019) 1064–1078.

[42] E. Casalone, A. Allione, C. Viberti, B. Pardini, S. Guarrera, M. Betti, I. Dianzani, E. Aldieri, G. Matullo, DNA methylation profiling of asbestos-treated MeT5A cell line reveals novel pathways implicated in asbestos response, Arch. Toxicol. 92 (5) (2018) 1785–1795.

[43] N. Usami, T. Fukui, M. Kondo, T. Taniguchi, T. Yokoyama, S. Mori, K. Yokoi, Y. Horio, K. Shimokata, Y. Sekido, T. Hida, Establishment and characterization of four malignant pleural mesothelioma cell lines from Japanese patients, Cancer Sci. 97 (5) (2006) 387–394.

[44] X. Rao, X. Huang, Z. Zhou, X. Lin, An improvement of the 2^(-delta delta CT) method for quantitative real-time polymerase chain reaction data analysis, Biostat. Bioinforma. Biomath. 3 (3) (2013) 71–85.

[45] S.H. Chew, Y. Okazaki, S. Akatsuka, S. Wang, L. Jiang, Y. Ohara, F. Ito, H. Saya, Y. Sekido, S. Toyokuni, Rheostatic CD44 isoform expression and its association with oxidative stress in human malignant mesothelioma, Free Radic. Biol. Med. 106 (2017) 91–99.

[46] T. Hirayama, H. Tsuboi, M. Niwa, A. Miki, S. Kadota, Y. Ikeshita, K. Okuda, H. Nagasawa, A universal fluorogenic switch for Fe(ii) ion based on N-oxide chemistry permits the visualization of intracellular redox equilibrium shift towards labile iron in hypoxic tumor cells, Chem. Sci. 8 (7) (2017) 4858–4866.

[47] S. Toyokuni, S. Okada, S. Hamazaki, M. Fujioka, J.L. Li, O. Midorikawa, Cirrhosis of the liver induced by cupric nitrilotriacetate in Wistar rats. An experimental model of copper toxicosis, Am. J. Pathol. 134 (6) (1989) 1263–1274.

[48] A.J. Valente, L.A. Maddalena, E.L. Robb, F. Moradi, J.A. Stuart, A simple ImageJ macro tool for analyzing mitochondrial network morphology in mammalian cell culture, Acta Histochem. 119 (3) (2017) 315–326.

[49] L. Jiang, Y. Yamashita, S.H. Chew, S. Akatsuka, S. Ukai, S. Wang, H. Nagai, Y. Okazaki, T. Takahashi, S. Toyokuni, Connective tissue growth factor and β-catenin constitute an autocrine loop for activation in rat sarcomatoid mesothelioma, J. Pathol. 233 (2014) 402–414.

[50] M.I. Koukourakis, A. Giatromanolaki, E. Sivridis, K. Simopoulos, J. Pastorek, C.C. Wykoff, K.C. Gatter, A.L. Harris, Hypoxia-regulated carbonic anhydrase-9 (CA9) relates to poor vascularization and resistance of squamous cell head and neck cancer to chemoradiotherapy, Clin. Cancer Res. 7 (11) (2001) 3399–3403.

[51] B.G. Wouters, J.M. Brown, Cells at intermediate oxygen levels can be more important than the "hypoxic fraction" in determining tumor response to fractionated radiotherapy, Radiat. Res. 147 (5) (1997) 541–550.

[52] Y. Lou, P.C. McDonald, A. Oloumi, S. Chia, C. Ostlund, A. Ahmadi, A. Kyle, U. Auf dem Keller, S. Leung, D. Huntsman, B. Clarke, B.W. Sutherland, D. Waterhouse, M. Bally, C. Roskelley, C.M. Overall, A. Minchinton, F. Pacchiano, F. Carta, A. Scozzafava, N. Touisni, J.Y. Winum, C.T. Supuran, S. Dedhar, Targeting tumor hypoxia: suppression of breast tumor growth and metastasis by novel carbonic anhydrase IX inhibitors, Cancer Res. 71 (9) (2011) 3364–3376.

[53] H.H. Hektoen, A.H. Ree, K.R. Redalen, K. Flatmark, Sulfamate inhibitor S4 influences carbonic anhydrase IX ectodomain shedding in colorectal carcinoma cells, J. Enzym. Inhib. Med. Chem. 31 (5) (2016) 779–786.

[54] E. Svastova, W. Witarski, L. Csaderova, I. Kosik, L. Skvarkova, A. Hulikova, M. Zatovicova, M. Barathova, J. Kopacek, J. Pastorek, S. Pastorekova, Carbonic anhydrase IX interacts with bicarbonate transporters in lamellipodia and increases cell migration via its catalytic domain, J. Biol. Chem. 287 (5) (2012) 3392–3402.

[55] M. Gao, P. Monian, Q. Pan, W. Zhang, J. Xiang, X. Jiang, Ferroptosis is an autophagic cell death process, Cell Res. 26 (9) (2016) 1021–1032.

[56] B.R. Stockwell, J.P. Friedmann Angeli, H. Bayir, A.I. Bush, M. Conrad, S.J. Dixon, S. Fulda, S. Gascon, S.K. Hatzios, V.E. Kagan, K. Noel, X. Jiang, A. Linkermann, M.E. Murphy, M. Overholtzer, A. Oyagi, G.C. Pagnussat, J. Park, Q. Ran, C.S. Rosenfeld, K. Salnikow, D. Tang, F.M. Torti, S.V. Torti, S. Toyokuni, K.A. Woerpel, D.D. Zhang, Ferroptosis: a regulated cell death nexus linking metabolism, redox biology, and disease, Cell 171 (2) (2017) 273–285.

[57] W. Hou, Y. Xie, X. Song, X. Sun, M.T. Lotze, H.J. Zeh 3rd, R. Kang, D. Tang, Autophagy promotes ferroptosis by degradation of ferritin, Autophagy 12 (8) (2016) 1425–1428.

[58] S.J. Dixon, K.M. Lemberg, M.R. Lamprecht, R. Skouta, E.M. Zaitsev, C.E. Gleason, D.N. Patel, A.J. Bauer, A.M. Cantley, W.S. Yang, Ferroptosis: an iron-dependent form of nonapoptotic cell death, Cell 149 (5) (2012) 1060–1072.

[59] A.M. van der Bliek, Q. Shen, S. Kawajiri, Mechanisms of mitochondrial fission and fusion, Cold Spring Harb. Perspect. Biol. 5 (6) (2013) a011072.

[60] S. Toyokuni, Iron-induced carcinogenesis: the role of redox regulation, Free Radic. Biol. Med. 20 (1996) 553–566.

[61] S. Toyokuni, Oxidative stress as an iceberg in carcinogenesis and cancer biology, Arch. Biochem. Biophys. 595 (2016) 46–49.

[62] Z.R. Chalmers, C.F. Connelly, D. Fabrizio, L. Gay, S.M. Ali, R. Ennis, A. Schrock, B. Campbell, A. Shlien, J. Chmielecki, F. Huang, Y. He, J. Sun, U. Tabori, M. Kennedy, D.S. Lieber, S. Roels, J. White, G.A. Otto, J.S. Ross, L. Garraway, V.A. Miller, P.J. Stephens, G.M. Frampton, Analysis of 100,000 human cancer genomes reveals the landscape of tumor mutational burden, Genome Med. 9 (1) (2017) 34.

[63] S. Nyholm, G.J. Mann, A.G. Johansson, R.J. Bergeron, A. Graslund, L. Thelander, Role of ribonucleotide reductase in inhibition of mammalian cell growth by potent iron chelators, J. Biol. Chem. 268 (35) (1993) 26200–26205.

[64] K.R. Olson, K.D. Straub, The role of hydrogen sulfide in evolution and the evolution of hydrogen sulfide in metabolism and signaling, Physiology 31 (1) (2016) 60–72.

[65] T. Mukaide, Y. Hattori, N. Misawa, S. Funahashi, L. Jiang, T. Hirayama, H. Nagasawa, S. Toyokuni, Histological detection of catalytic ferrous iron with the selective turn-on fluorescent probe RhoNox-1 in a Fenton reaction-based rat renal carcinogenesis model, Free Radic. Res. 48 (2014) 990–995.

[66] T. Hirayama, H. Nagasawa, Chemical tools for detecting Fe ions, J. Clin. Biochem. Nutr. 60 (1) (2017) 39–48.

[67] T. Hirayama, Fluorescent probes for the detection of catalytic Fe(II) ion, Free Radic.

Biol. Med. 133 (2019) 38–45.
[68] J.P. Liuzzi, F. Aydemir, H. Nam, M.D. Knutson, R.J. Cousins, Zip 14 (Slc39a14) mediates non-transferrin-bound iron uptake into cells, Proc. Natl. Acad. Sci. U. S. A. 103 (37) (2006) 13612–13617.
[69] S. Tandy, M. Williams, A. Leggett, M. Lopez-Jimenez, M. Dedes, B. Ramesh, S.K. Srai, P. Sharp, Nramp2 expression is associated with pH-dependent iron uptake across the apical membrane of human intestinal Caco-2 cells, J. Biol. Chem. 275 (2) (2000) 1023–1029.
[70] H. Drakesmith, E. Nemeth, T. Ganz, Ironing out ferroportin, Cell Metabol. 22 (5) (2015) 777–787.
[71] M. Razi, E.Y. Chan, S.A. Tooze, Early endosomes and endosomal coatomer are required for autophagy, J. Cell Biol. 185 (2) (2009) 305–321.
[72] Y. Ikeda, A. Shirakabe, Y. Maejima, P. Zhai, S. Sciarretta, J. Toli, M. Nomura, K. Mihara, K. Egashira, M. Ohishi, M. Abdellatif, J. Sadoshima, Endogenous Drp1 mediates mitochondrial autophagy and protects the heart against energy stress, Circ. Res. 116 (2) (2015) 264–278.
[73] Q. Zheng, Y. Zhao, J. Guo, S. Zhao, C. Fei, C. Xiao, D. Wu, L. Wu, X. Li, C. Chang, Iron overload promotes mitochondrial fragmentation in mesenchymal stromal cells from myelodysplastic syndrome patients through activation of the AMPK/MFF/Drp1 pathway, Cell Death Dis. 9 (5) (2018) 515.
[74] L. Galluzzi, I. Vitale, S.A. Aaronson, J.M. Abrams, D. Adam, P. Agostinis, E.S. Alnemri, L. Altucci, I. Amelio, D.W. Andrews, M. Annicchiarico-Petruzzelli, A.V. Antonov, E. Arama, E.H. Baehrecke, N.A. Barlev, N.G. Bazan, F. Bernassola, M.J.M. Bertrand, K. Bianchi, M.V. Blagosklonny, K. Blomgren, C. Borner, P. Boya, C. Brenner, M. Campanella, E. Candi, D. Carmona-Gutierrez, F. Cecconi, F.K. Chan, N.S. Chandel, E.H. Cheng, J.E. Chipuk, J.A. Cidlowski, A. Ciechanover, G.M. Cohen, M. Conrad, J.R. Cubillos-Ruiz, P.E. Czabotar, V. D'Angiolella, T.M. Dawson, V.L. Dawson, V. De Laurenzi, R. De Maria, K.M. Debatin, R.J. DeBerardinis, M. Deshmukh, N. Di Daniele, F. Di Virgilio, V.M. Dixit, S.J. Dixon, C.S. Duckett, B.D. Dynlacht, W.S. El-Deiry, J.W. Elrod, G.M. Fimia, S. Fulda, A.J. Garcia-Saez, A.D. Garg, C. Garrido, E. Gavathiotis, P. Golstein, E. Gottlieb, D.R. Green, L.A. Greene, H. Gronemeyer, A. Gross, G. Hajnoczky, J.M. Hardwick, I.S. Harris, M.O. Hengartner, C. Hetz, H. Ichijo, M. Jaattela, B. Joseph, P.J. Jost, P.P. Juin, W.J. Kaiser, M. Karin, T. Kaufmann, O. Kepp, A. Kimchi, R.N. Kitsis, D.J. Klionsky, R.A. Knight, S. Kumar, S.W. Lee, J.J. Lemasters, B. Levine, A. Linkermann, S.A. Lipton, R.A. Lockshin, C. Lopez-Otin, S.W. Lowe, T. Luedde, E. Lugli, M. MacFarlane, F. Madeo, M. Malewicz, W. Malorni, G. Manic, J.C. Marine, S.J. Martin, J.C. Martinou, J.P. Medema, P. Mehlen, P. Meier, S. Melino, E.A. Miao, J.D. Molkentin, U.M. Moll, C. Munoz-Pinedo, S. Nagata, G. Nunez, A. Oberst, M. Oren, M. Overholtzer, M. Pagano, T. Panaretakis, M. Pasparakis, J.M. Penninger, D.M. Pereira, S. Pervaiz, M.E. Peter, M. Piacentini, P. Pinton, J.H.M. Prehn, H. Puthalakath, G.A. Rabinovich, M. Rehm, R. Rizzuto, C.M.P. Rodrigues, D.C. Rubinsztein, T. Rudel, K.M. Ryan, E. Sayan, L. Scorrano, F. Shao, Y. Shi, J. Silke, H.U. Simon, A. Sistigu, B.R. Stockwell, A. Strasser, G. Szabadkai, S.W.G. Tait, D. Tang, N. Tavernarakis, A. Thorburn, Y. Tsujimoto, B. Turk, T. Vanden Berghe, P. Vandenabeele, M.G. Vander Heiden, A. Villunger, H.W. Virgin, K.H. Vousden, D. Vucic, E.F. Wagner, H. Walczak, D. Wallach, Y. Wang, J.A. Wells, W. Wood, J. Yuan, Z. Zakeri, B. Zhivotovsky, L. Zitvogel, G. Melino, G. Kroemer, Molecular mechanisms of cell death: recommendations of the nomenclature committee on cell death 2018, Cell Death Differ. 25 (3) (2018) 486–541.
[75] S. Fossati, P. Giannoni, M.E. Solesio, S.L. Cocklin, E. Cabrera, J. Ghiso, A. Rostagno, The carbonic anhydrase inhibitor methazolamide prevents amyloid beta-induced mitochondrial dysfunction and caspase activation protecting neuronal and glial cells in vitro and in the mouse brain, Neurobiol. Dis. 86 (2016) 29–40.